RSC Advances

ROYAL SOCIETY OF CHEMISTRY

www.rsc.org/advances

Cite this: DOI: 10.1039/c0xx00000x

www.rsc.org/xxxxxx

ARTICLE TYPE

Graphene oxide/core-shell structured TiO_2@TiO_{2-x} nanocomposites with highly efficient visible-light photocatalytic performance

Shunhang Wei,[a] Rong Wu,[*a] Jikang Jian,[b] Juan Hou,[c] Fengjuan Chen,[a] Abduleziz Ablat[a] and Yanfei Sun[a]

Received (in XXX, XXX) Xth XXXXXXXXX 20XX, Accepted Xth XXXXXXXXX 20XX
DOI: 10.1039/b000000x

Graphene oxide/core-shell structured TiO_2@TiO_{2-x} nanocomposites with outstanding photocatalytic performance were prepared by combining graphene oxide and black titania we reported before. Amounts of Ti^{3+} and graphene oxide as a mediator of electron transfer were introduced into the compounds, which strongly enhanced visible-light absorption and photocatalysis.

Photocatalytic degradation of organic pollutants in water has attracted much attention. Photocatalysis based on semiconductors is considered to be a promising technology for pollution abatement, because semiconductors can potentially work under solar irradiation without generating harmful by-products.[1,2] Among the various semiconductor photocatalysts, TiO_2 is the most widely used photocatalyst for environmental purification because of its physical and chemical stability, nontoxicity, and low cost.[3] However, some drawbacks of conventional white TiO_2 limit its wide application. A wide band gap (3.2eV for anatase) results in poor visible absorption.[4] Also, the rapid electron-hole recombination of TiO_2 markedly limits photocatalytic oxidation of organic compounds on the surface.[5] Many methods have been developed to overcome these problems and enable efficient use of visible light. The presence of black TiO_2 with amounts of Ti^{3+} and oxygen vacancies largely solves these drawbacks, and exhibits strong visible-light absorption and low electron-hole recombination.[6-9] In particular, based on the results reported by Huang *et al.*, black titania with a core-shell structure performs better photocatalytic activity.[7,10] Although the photocatalytic degradation rate of black TiO_2 greatly increases under visible-light irradiation, the degradation time is still long because most black TiO_2 requires 3h to degrade around 40% of the concentration of contaminant after adsorption/desorption equilibrium.[7,11]

Recently, the incorporation of carbon material into TiO_2-based composite materials has been reported to enhance the photocatalytic activity in a number of studies.[12-15] Graphene oxide (GO) as one of carbon material (chemically modified graphene with hydroxyl and carboxyl groups) has large specific surface area and high activity in most catalytic processes, which provides fertile opportunities for the construction of graphene oxide-based hybrid nanocomposites.[16] In addition, GO is negatively charged, hydrophilic, and readily disperses in water to form a stable colloidal suspension.[17] Hence, GO-based hybrid photocatalysts currently attract much attentions for photodegradation. Several hybridized GO and TiO_2 have recently been reported to significantly enhance the photocatalytic performance in the degradation of pollutants [18-20].

Herein for the first time we show a new facile method to prepare GO/core-shell structured TiO_2@TiO_{2-x} nanocomposites with excellent photodegradation efficiency under visible-light irradiation. In this method, the colloid as titania precursor was prepared by a previously reported preparation method for black titania.[9] The composite material is obtained by heating a mixture of the colloid and GO. The one annealed in N_2 atmosphere is designated as GT(N_2), whereas the other one annealed in air is GT(air). It exhibits not only high photodegradation efficiency, but also excellent visible-light absorption.

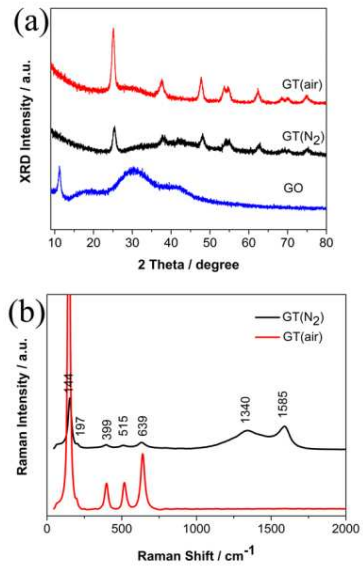

Fig. 1 XRD patterns (a) and Raman spectra (b) of GT(N_2) and GT(air)

The X-ray diffraction (XRD) patterns of the GO-TiO_2 samples are shown in Fig. 1a. The diffraction peaks at 25.2°, 37.8°, 47.9°, 54°, 55°, 62.7°, 68.8°, 70.2° and 75° are assigned to the (1 0 1), (0 0 4), (2 0 0), (1 0 5), (2 1 1), (2 0 4), (1 1 6), (2 2 0) and (2 1 5) reflections of anatase TiO_2, respectively. The diffraction peak at around 42.1° for GT(N_2) is ascribed to GO. However, no diffraction peaks of GO are present for GT(air). The structural characteristics of the two samples were further investigated by Raman spectroscopy, as shown in Fig. 1b. The Raman spectra unambiguously indicate that both samples contain typical anatase TiO_2. For GT(N_2) sample, the D band (~1340 cm^{-1}) originating from defects such as disordered carbon and the G band (~1585 cm^{-1}) corresponding to sp^2 bonded carbon are observed.[21] Hence, GT(N_2) is a successful compound sample of GO and anatase TiO_2. In contrast, the absence of the D and G bands in the GT(air) spectrum indicate composite failure. It may be ascribed to intense

disruption of GO in GT(air), which leads to C doping in TiO_2 rather than formation of a GO-TiO_2 compound.

The morphology of the as-prepared GT(N_2) and GT(air) samples were characterized by TEM (Fig. 2a and c). Clearly, for the GT(N_2) nanoparticles, TiO_2 is uniformly deposited on the surface of GO. In contrast, only TiO_2 can be seen in GT(air). The high resolution transmission electron microscopy (HRTEM) (Fig.2b and d) images show clear lattice fringes and fringe spacing of 0.35 nm matching up with the (101) crystallographic plane of anatase TiO_2. The corresponding fast Fourier transform (FFT) image also shows only TiO_2 in the GT(air) sample. The results also show the failure of composite of GO and TiO_2 in GT(air). Interestingly, a unique core – shell structure (a disordered surface coating a crystalline core) can be seen in the two samples. The disordered shell is marked out by blue arrows, and may possess a looser structure than the crystalline core.[11] In addition, the disordered shell in GT(N_2) is thicker than that in GT(air).

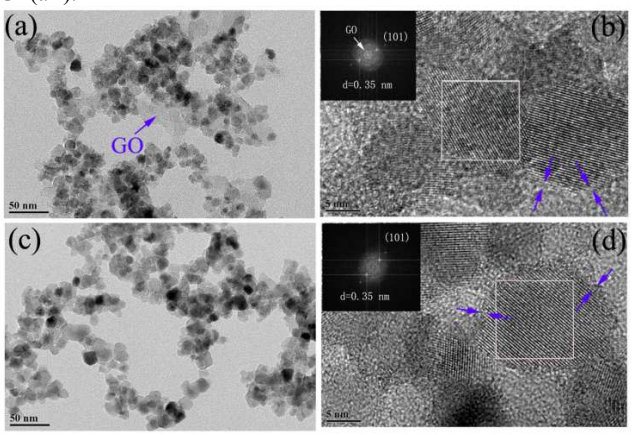

Fig. 2 (a) TEM image of GT(N_2). (b) HRTEM micrographs of GT(N_2). (c) TEM image of GT(air). (d) HRTEM micrographs of GT(air).

FTIR spectra of GT(air) and GT(N_2) are illustrated in Fig. 3a. The peaks at around 3378 and 1625 cm^{-1} are attributed to stretching and bending vibrations of hydroxyl groups, respectively.[22] The peak at around 1550 cm^{-1} is associated with the formation of $–COO^-$ after coating with TiO_2.[21] The peak at around 1185 cm^{-1} is attributed to stretching of C-OH.

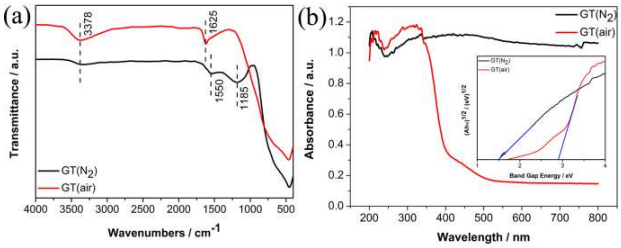

Fig. 3 FTIR spectra (a) and Spectral absorbance (b) of GT(N_2) and GT(air)

The UV-vis absorption spectra of GT(N_2) and GT(air) nanocomposites are investigated. As shown in Fig. 3b, both the as-prepared samples exhibit strong absorption of visible-light. The absorption edges of GT(N_2) show a significant red shift to around 756 nm , which is attributed to the bonding effect between graphene oxide and TiO_2. As can be seen clearly, the introduction of GO into the matrix of GT(N_2) is able to effectively promote visible light absorption of the nanocomposite, which can be ascribed to electronic interactions between GO and TiO_2.[23] In addition, based on previous research, the introduction of Ti^{3+} and oxygen vacancies can enhance light absorption.[9,11] Hence, additional characterizations were performed to confirm the existence of Ti^{3+} and oxygen vacancies in the samples.

Electron paramagnetic resonance (EPR) is widely used to characterize the existence of Ti^{3+} and oxygen vacancies, because it is highly sensitive to detect paramagnetic species containing unpaired electrons. Fig. S1 (ESI) shows the room temperature EPR results of GT(N_2) and GT(air). The sharp strong signal at a *g*-value of ~2.002 can be attributed to surface Ti^{3+}.[24] Given that the signal area is proportional to the amount of Ti^{3+}, it can be concluded that GT(N_2) has larger amounts of Ti^{3+} and oxygen vacancies than GT(air).

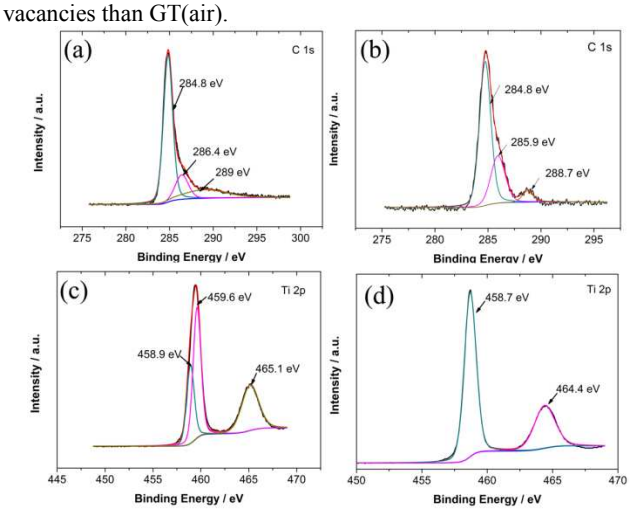

Fig. 4 XPS spectra for (a) C 1s of GT(N_2), (b) C 1s of GT(air), (c) Ti 2p of GT(N_2) and Ti 2p of GT(air).

The elemental and chemical states of GT(N_2) and GT(air) were investigated using X-ray photoelectron spectroscopy (XPS). The C 1s spectrum of GT(N_2) (Fig. 4a) is fitted into three peaks located at 284.8 eV, 286.4 eV and 289 eV, respectively, while that for GT(air) (Fig. 4b) is 284.8 eV, 285.9 eV and 288.7 eV. The peak at 284.8 eV is attributed to C-C corresponding to sp^2 hybridized structures. The binding energy of 286.4 eV is typically assigned to C-OH.[25] Another peak located at 289 eV is assigned to HO–C=O.[25] Compared with the GT(air) spectrum, the positions of the C-OH and HO-C=O peaks obviously shift from 286.4 eV to 285.9 eV, and 289 eV to 288.7eV, respectively. The phenomenon indicates that the OH groups on the surface of TiO_2 possibly reacted with the C−OH and COOH groups on the GO surface through dehydration to form C−O−Ti and O=C−O−Ti bonds, respectively.[26,27] The results prove our deduction that C doping into TiO_2 through intense disruption of GO annealed in air. In addition, the atomic percentage of C atoms in GT(N_2) and GT(air) were about 44.24 wt.% and 19.81 wt.%, respectively (Fig.S2 in ESI). Fig. 4d shows XPS spectrum of GT(air) in the Ti 2p binding energy region. The two peaks at 458.7 eV and 464.4 eV are attributed to the Ti^{4+} chemical state. In contrast, the XPS spectrum of GT(N_2) (Fig. 4c) can be fitted to three binding energies. The peak located at 459.6 eV is assigned to formation of Ti-C bonds on the sample surface.[27] In addition, the binding energies of Ti 2p1/2, Ti 2p3/2 and O 1s (Fig.S3 in ESI) of GT(N_2) are upward shifted. It indicates the insertion of Ti^{4+} cations into the layered sites of GO network to form Ti–O–C linkages.[28] The shortening of the Ti–O bonds leads to an increase of the binding energy of the O atom. Moreover, the decrease of electron density around the Ti atom results in an increase of the binding energy of Ti, because the electronegativity of C is greater than that of Ti.[28,29] However, no peaks of Ti^{3+} are present in the GT(N_2) and GT(air) samples, which may be subjected to the

detection distance (ten atomic layers) for XPS.[7] Hence, the core – shell structure can be ascribed to TiO_2 @ TiO_{2-x}.

Photoluminescence (PL) measurements were applied to understand the separation and recombination of photogenerated charge carriers, and to reveal the transfer of photogenerated electrons and holes. Fig. S4 (ESI) shows the PL spectra of GT(N_2) and GT(air) under 240 nm light excitation at room temperature. It is clear that the PL intensity of GT(N_2) is much lower than that of GT(air), which indicates an increase in the electron-hole separation rate resulting in higher photocatalytic activity. Hence, the introduction of GO is good for increasing the charge separation efficiency.

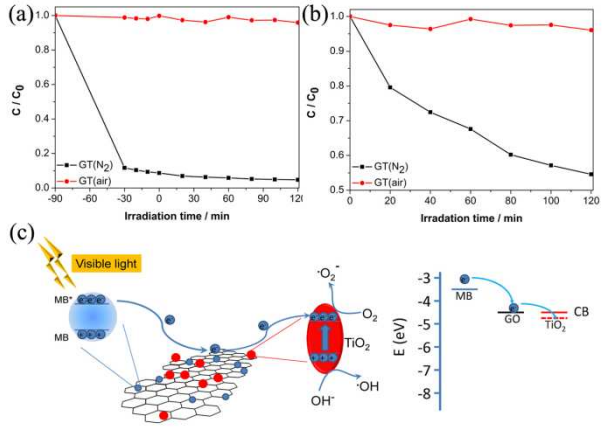

Fig. 5 (a) Photodegradation of MB in 120 min over GT(N_2) and GT(air), (b) Comparison of MB degradation over different samples under visible light (absorbance at a particular time and that at initial concentration of MB after adsorption equilibrium are denoted as C and C_0, respectively.), (c) Schematic diagrams of the photoinduced charge separation and migration processes

Methylene blue (MB)(40mg/L) was selected to evaluate the photocatalytic activity of the catalysts. It is well known that adsorption of organic molecules to the compound surface is an essential step in photocatalytic degradation. Thus it is vital to investigate the adsorption characteristic of MB onto the surface of the different samples. As shown in Fig. 5a, most dye molecules remain in the solution with GT(air) as the catalyst after adsorption/desorption equilibrium in the dark for 90 min, whereas a large amount of dye molecules are adsorbed on the surface of the GT(N_2) sample (see Table S1 in ESI†). Fig. 5b shows the degradation/removal of MB under visible light irradiation. The GT(N_2) sample exhibits higher photocatalytic activity than the GT(air) sample. For GT(N_2), the degradation of MB reached 45.4% after irradiation for 120 minutes with visible light, whereas GT(air) only decomposed about 4% of the MB. Hence, compared with sole black titania, the degradation rate of the composite has greatly improved.

These results show the excellent photocatalytic performance of GT(N_2) under visible light irradiation. The improved photocatalytic performance can be assigned to the enhanced light harvesting and more efficient separation of photogenerated electron–hole pairs. Fig. 5c illustrates a mechanistic profile of the photoinduced charge separation and migration process. Considering the potential of the conduction band (CB) of bare anatase TiO_2 (–4.42 eV vs. vacuum), MB (–3.60 eV) and GO (-4.42 eV), photoinduced electrons from excited MB absorbed on GO can hardly transfer from the GO sheet to TiO_2.[23,30] However, when TiO_2 is strongly bonded to the surface of the GO sheet, the band narrowing (3.2 eV – 1.5 eV) of TiO_2 in the GO-TiO_2 sample will change the energy difference between GO and TiO_2 to allow electrons from the excited MB to flow to the conduction band of TiO_2 via GO.[31,32] These electron transfers could significantly suppress the recombination of electrons from excited MB, which result in enhancement of self-degradation and photocatalytic degradation. Meanwhile, the formation of lots of Ti^{3+} and oxygen vacancies effectively promotes electrons in the valence band to be excited to the conduction band of TiO_2 and inhibit the recombination of e^-/h^+ pairs.[33-37] The electrons accumulated on the surface of TiO_2 are then trapped by dissolved oxygen molecules in aqueous solution to yield highly oxidative species such as the superoxide radical anion and hydroxyl radical, which can oxidative decomposition of MB effectively. In addition, the electrostatic attractions between positively charged MB and negatively charged GO promote the adsorption and make the contact between MB and TiO_2 better, which also accelerates the decomposition. However, The presence of Ti^{3+} does not promote the photocatalytic performance of GT(air). It can be ascribed to the insufficient amount of Ti^{3+}, which creates localized oxygen vacancy states below the H_2/H_2O redox potential that actually reduces the electron mobility and exhibit negligible visible photoactivity. [9,38]

Conclusions

In conclusion, graphene oxide/core-shell structured TiO_2@TiO_{2-x} nanocomposites with high adsorption and visible-light photocatalytic performance were prepared by a new chemical approach. The low recombination rate of photogenerated electron–hole pairs and strongly enhanced visible-light absorption can be attributed to two factors: (1) the introduction of large amounts of Ti^{3+} and (2) graphene oxide as mediation of electron transfer. The method may provide a new way to improve water cleaning applications.

Notes and references

This work was financially supported by the National Natural Science Foundation of China (No.11164026, 51362026, 51472052, 61464010)

[a] Key Laboratory of Solid-state Physics and Devices, School of Physical Science and Technology, Xinjiang University ,Urumqi830046,China. Email: wurongxju@sina.com
[b] School of Physics and Optoelectronic Engineering, Guangdong University of Technology, WaiHuan Xi Road, No. 100, Guangzhou 510006, China
[c] Key Laboratory of Ecophysics and Department of Physics, School of Science, Shihezi University, Xinjiang 832003, China

† Electronic Supplementary Information (ESI) available: Experimental details, EPR, XPS, PL, and Physical and Structural Properties of samples

1 A. Mills, R. H. Davies and D. Worsley, *Chem. Soc. Rev.*, 1993, 22, 417.
2 M. R. Hoffmann，S. T. Martin，W. Y. Choi and D.W. Bahnemann, *Chem. Rev.*,1995, 95, 69.
3 X. Chen and S.S. Mao, *Chemical Reviews*, 2007, 107, 2891.
4 R. Asahi, T. Morikawa, T. Ohwaki, K. Aoki and Y. Taga, *Science*, 2001, 293, 269.
5 J.M. Herrmann, *Catalysis Today*, 1999, 53, 115.
6 X.B. Chen, L. Liu, P.Y. Yu and S.S. Mao, *Science*, 2011, 331, 746.
7 Z. Wang, C.Y. Yang, T.Q. Lin, H. Yin, P. Chen, D.Y. Wan, F.F. Xu, F.Q. Huang, J.H. Lin, X.M. Xie and M.H. Jiang, *Energy & Environmental Science*, 2013, 6, 3007.
8 S.T. Myung, M. Kikuchi, C.S. Yoon, H. Yashiro, S.J. Kim, Y.K. Sun and B. Scrosati, *Energy & Environmental Science*, 2013, 6, 2609.
9 S.H. Wei, R. Wu, J.K. Jian, F.J. Chen, Y.F. Sun, *Dalton Trans.*, 2015, 44 (4), 1534.
10 T.Q. Lin, C.Y. Yang, Z. Wang, H. Yin, X.J. Lv, F.Q. Huang, J.H. Lin,

X.M. Xie and M.H. Jiang, *Energy Environ. Sci.* 2014,7, 967.
11 G.L. Zhu, T.Q. Lin, X.J. Lu, W. Zhao, C.Y. Yang, Z. Wang, H. Yin, Z.Q. Liu, F.Q. Huang and J.H. Lin, *Journal of Materials Chemistry A*, 2013, 1, 9650.
12 R. Leary and A. Westwood, *Carbon*, 2011, 49, 741.
13 K. Woan, G. Pyrgiotakis and W. Sigmund, *Advanced Materials*, 2009, 21, 2233.
14 H. Zhang, X.J. Lv, Y.M. Li, Y. Wang and J.H. Li, *Acs Nano*, 2010, 4, 380.
15 Q.J. Xiang, J.G. Yu and M. Jaroniec, *Chemical Society Reviews*, 2012, 41, 782.
16 D.A. Dikin, S. Stankovich, E.J. Zimney, R.D. Piner, G.H.B. Dommett, G. Evmenenko, S.T. Nguyen and R.S. Ruoff, *Nature*, 2007, 448, 457.
17 H.F. Yang, F.H. Li, C.S. Shan, D.X. Han, Q.X. Zhang, L. Niu and A. Ivaska, *Journal of Materials Chemistry*, 2009, 19, 4632.
18 J. Du, X.Y. Lai, N.L. Yang, J. Zhai, D. Kisailus, F.B. Su, D. Wang and L. Jiang, *Acs Nano*, 2011, 5, 590.
19 P. Song, X.Y. Zhang, M.X. Sun, X.L. Cui, Y.H. Lin, *Nanoscale*, 2012, 4, 1800.
20 J.Y. Jing, Y. Zhang, W.Y. Li and W.W. Yu, *Journal of Catalysis*, 2014, 316, 174.
21 L. Z. Bai, D. L. Zhao, Y. Xu, J. M. Zhang, Y. L. Gao, L. Y. Zhao and J. T. Tang, *Materials Letters*, 2012, 68, 399.
22 J. Fang, F.C. Shi, J. Bu, J.J. Ding, S.T. Xu, J. Bao, Y.S. Ma, Z.Q. Jiang, W.P. Zhang, C. Gao and W.X. Huang, *Journal of Physical Chemistry C*, 2010, 114, 7940.
23 L. Liu, H.W. Bai, J.C. Liu and D.D. Sun, *Journal of Hazardous Materials*, 2013, 261, 214.
24 A.L. Attwood, D.M. Murphy, J.L. Edwards, T.A. Egerton and R.W. Harrison, *Research on Chemical Intermediates*, 2003, 29, 449.
25 J.Y. Jing, Y. Zhang, W.Y. Li and W.W. Yu, *Journal of Catalysis*, 2014, 316, 174.
26 S. Ponce, M.A. Pena and J.L.G. Fierro, *Applied Catalysis B-Environmental*, 2000, 24, 193.
27 X.N. Lu, C.Y. Song, C.C. Chang, Y.X. Teng, Z.S. Tong and X.L. Tang, *Industrial & Engineering Chemistry Research*, 2014, 53, 11601.
28 Z.J. Li, B. Hou, Y. Xu, D. Wu and Y.H. Sun, *Journal of Colloid and Interface Science*, 2005, 288, 149.
29 X.L. Yan, J. He, D.G. Evans, X. Duan and Y.X. Zhu, *Applied Catalysis B-Environmental*, 2005, 55, 243.
30 J.T. Zhang, Z.G. Xiong and X.S. Zhao, *Journal of Materials Chemistry*, 2011, 21, 3634.
31 Y.R. Ni, W. Wang, W.J. Huang, C.H. Lu and Z.Z. Xu, *Journal of Colloid and Interface Science*, 2014, 428, 162.
32 J.S. Lee, K.H. You and C.B. Park, *Advanced Materials*, 2012, 24, 1084.
33 J.X. Li, J.H. Xu, W.L. Dai and K.N. Fan, *Journal of Physical Chemistry C*, 2009, 113, 8343.
34 H.B. Zeng, G.T. Duan, Y. Li, S.K. Yang, X.X. Xu and W.P. Cai, *Advanced Functional Materials*, 2010, 20, 561.
35 H.B. Zeng, W.P. Cai, P.S. Liu, X.X. Xu, H.J. Zhou, C. Klingshirn and H. Kalt, *ACS Nano*, 2008, 2, 1661.
36 X.J. Lv, W.G. Yang, Z.W. Quan, T.Q. Lin, L.G. Bai, L. Wang, F.Q. Huang and Y.S. Zhao, *J. Am. Chem. Soc.*, 2014, 136, 419.
37 X.J. Lv, X.L. Mou, Y.M. Wang, F.Q. Huang and F.F. Xu, *Adv. Mater.*,2010, 22, 3719.
38 I. Justicia, P. Ordejon, G. Canto, J.L. Mozos, J. Fraxedas, G.A. Battiston, R. Gerbasi and A. Figueras, *Advanced Materials*, 2002, 14, 1399.